PHYSICAL REVIEW A **69**, 050101(R) (2004)

Effects of confinement on the permanent electric-dipole moment of Xe atoms in liquid Xe

Boris Ravaine and Andrei Derevianko
Department of Physics, University of Nevada, Reno, Nevada 89557, USA
(Received 16 October 2003; published 25 May 2004)

Searches for permanent electric-dipole moments (EDM) of atoms provide important constraints on competing extensions to the standard model of elementary particles. Recently proposed experiment with liquid ^{129}Xe [M.V. Romalis and M.P. Ledbetter, Phys. Rev. Lett. **87**, 067601 (2001)] may significantly improve present limits on the EDMs. To interpret experimental data in terms of *CP*-violating sources, one must relate measured atomic EDM to various model interactions via electronic-structure calculations. Here we study density dependence of atomic EDMs. The analysis is carried out in the framework of the cell model of the liquid coupled with relativistic atomic-structure calculations. We find that compared to an isolated atom, the EDM of an atom of liquid Xe is suppressed by about 40%.

DOI: 10.1103/PhysRevA.69.050101 PACS number(s): 11.30.Er, 32.10.Dk, 61.20.Ja, 31.30.Jv

Most extensions of the standard model of elementary particles, e.g., supersymmetry, naturally produce permanent electric dipole moments (EDM) of atoms and molecules [1] that are comparable to or larger than present limits (see, e.g., a popular review [2]). For example, the most accurate to date determination of atomic EDM of ^{199}Hg [3] sets limits on a number of important parameters: *CP*-violating QCD vacuum angle, quark chromo-EDMs, and semileptonic *CP*-violating parameters, and it restricts parameter space for certain extensions to the standard model. A substantial, several orders of magnitude improvement in sensitivity to all the enumerated sources of *CP* violation is anticipated in an experiment proposed by Romalis and Ledbetter [4]. These authors propose to search for an EDM of a liquid sample of ^{129}Xe. Compared to the gas-phase experiment [5], a drastically improved sensitivity of the liquid Xe experiment is mainly due to the higher number densities of the liquid phase (10^{22} atoms/cm^3).

The very use of the liquid phase raises questions about density-dependent factors which can influence the outcome and interpretation of the experiment. For example, an EDM experiment with a molecular liquid was proposed in Ref. [6]. The authors found an additional suppression of the EDM signal by a factor of 100 due to a reduced population of molecular rotational levels in liquid. Although the experiment with liquid Xe will be free from such an effect, it is clear that the effects of the liquid phase on atomic EDMs have to be investigated.

An EDM of an atom is related to a strength of a *CP*-violating source via electronic-structure (enhancement or shielding) factors. For an isolated Xe atom such factors were computed previously: *P*,*T*-odd semileptonic interactions were considered by Mårtensson-Pendrill [7] and the nuclear Schiff moment by Dzuba *et al.* [8]. Here we employ a simple cell model to study density dependence of the electronic-structure factors. Technically, we extend the previous atomic relativistic many-body calculations by confining a Xe atom to a spherically symmetric cavity. In a nonpolar liquid such as liquid Xe, this cavity roughly approximates an averaged interaction with the neighboring atoms. Imposing proper boundary conditions at the cavity radius, first we solve the Dirac-Hartree-Fock (DHF) equations and then employ the more sophisticated relativistic random-phase approximation (RRPA) to account for correlations. We find that compared to the EDM of an isolated atom, the resulting EDM of an atom of liquid Xe is suppressed by about 40%. Thus if the experiment with liquid Xe is carried out with the anticipated sensitivity, we expect that the inferred constraints on possible sources of *CP* violation would indeed be several orders of magnitude more stringent than the present limits.

Sources of atomic EDM. The conventional atomic Hamiltonian H_0 among other symmetries is invariant with respect to space reflection (P) and time reversal (T). Therefore, on very general grounds, an expectation value of the electric dipole operator $\mathbf{D}=-\Sigma_i \mathbf{r}_i$ in a nondegenerate atomic state $|\Psi_0\rangle$ vanishes. The tiny *CP*-violating interactions, here generically denoted as $H_{CP}=\Sigma_i h_{CP}(\mathbf{r}_i)$, break the symmetry of the atom and induce a correction to the electronic state $|\tilde{\Psi}\rangle = |\Psi_0\rangle + |\delta\Psi\rangle$. To the lowest order

$$|\delta\Psi\rangle = \sum_k |\Psi_k\rangle \frac{\langle\Psi_k|H_{CP}|\Psi_0\rangle}{E_0 - E_k}, \tag{1}$$

where E_k and $|\Psi_k\rangle$ are eigenvalues and eigenfunctions of H_0. Due to selection rules, the $|\delta\Psi\rangle$ admixture has a parity opposite to the one of the reference state $|\Psi_0\rangle$. Because of this opposite-parity admixture the atom acquires a permanent EDM

$$\mathbf{d} = \langle\tilde{\Psi}|\mathbf{D}|\tilde{\Psi}\rangle = 2\langle\Psi_0|\mathbf{D}|\delta\Psi\rangle. \tag{2}$$

Now we specify particular forms of H_{CP}. An analysis [1] shows that for diamagnetic atoms, such as Xe, the EDM predominantly arises due to *P*,*T*-odd semileptonic interaction H_{TN} between electrons and nucleons and also due to interaction H_{SM} of electrons with the so-called nuclear Schiff moment [9]. Smaller atomic EDM is generated by intrinsic EDM of electrons and we will not consider this mechanism here. Atomic units $|e|=\hbar=m_e=4\pi\varepsilon_0\equiv 1$ are used throughout.

Explicitly, the effective *P*,*T*-odd semileptonic interaction Hamiltonian may be represented as [7]

$$h_{\mathrm{TN}}(\mathbf{r}_e) = \sqrt{2} G_F C_{\mathrm{TN}} \boldsymbol{\sigma}_N \cdot (i\gamma_0\gamma_5\boldsymbol{\sigma})_e \rho_N(\mathbf{r}_e). \quad (3)$$

Here subscripts e and N distinguish between operators acting in the space of electronic and nuclear coordinates, respectively. C_{TN} is a coupling constant to be determined from an interpretation of EDM measurements and to be compared with theoretical model-dependent predictions. Due to averaging over nuclear degrees of freedom, this interaction depends on nuclear density distribution $\rho_N(r)$. In the following, we approximate $\rho_N(r)$ as a Fermi distribution $\rho_N(r) = \rho_0/\{1 + \exp[(r-c)/a]\}$, with $c = 5.6315$ fm and $a = 0.52$ fm. Finally, $G_{\mathrm{F}} \approx 2.22254 \times 10^{-14}$ a.u. is the Fermi constant.

The interaction of an electron with the nuclear Schiff moment $\mathbf{S}$ has the form [10]

$$h_{\mathrm{SM}}(\mathbf{r}_e) = \frac{3}{B_4} \rho_N(\mathbf{r}_e)(\mathbf{r}_e \cdot \mathbf{S}), \quad (4)$$

where $B_4 = \int_0^\infty r^4 \rho_N(r) dr$ is the fourth-order moment of the nuclear distribution. The Schiff moment characterizes a difference between charge and EDM distributions inside the nucleus. It depends on a number of important *CP*-violating parameters enumerated in the introduction.

Finally, we emphasize that both H_{TN} and H_{SM} are contact interactions. They occur when an electron penetrates the nucleus. The electron speed at the nucleus is approximately $\alpha Z c \simeq \frac{1}{2} c (Z = 54)$, i.e., a fully relativistic description of electronic motion is important in this problem.

Cell model of liquid xenon. Here we employ a simple cell model (see [11] and references therein) to estimate the effects of the environment on permanent EDM of a given atom. According to the cell model, we confine an atom to a spherical cavity of radius

$$R_{\mathrm{cav}} = \left(\frac{3}{4\pi} \frac{1}{n} \right)^{1/3}, \quad (5)$$

n being the number density of the sample. For a density of liquid Xe of 500 amagat [12], $R_{\mathrm{cav}} \simeq 4.9$ bohr. In nonrelativistic calculations, periodicity requires that the normal component of the gradient of electronic wave function vanishes at the surface of the cell (see, e.g., [13])

$$\frac{\partial \Psi}{\partial r}(R_{\mathrm{cav}}) = 0. \quad (6)$$

Before proceeding with a technical question of implementing these boundary conditions in relativistic calculations, we notice that the cell model implicitly incorporates an average polarization interaction with the media. Indeed, the Hamiltonian of an atom placed in the liquid in addition to the conventional atomic Hamiltonian H_0 includes the interaction of electrons with the rest of the atoms in the media. This interaction is dominated by polarization potential. An important point is that the *averaged* polarization interaction can be expressed as $V_p = -\frac{1}{2}(1 - \epsilon^{-1}) R_{\mathrm{cav}}^{-1}$, where ϵ is the dielectric constant of the media [13]. This interaction does not depend on an electronic coordinate — it is just an additive constant that does not affect calculations of EDM. Thus we may approximate the total Hamiltonian with the traditional atomic Hamiltonian H_0.

Furthermore, the spherical symmetry of the cell allows us to employ traditional methods of atomic structure. The only modification is due to boundary conditions (6). However, in relativistic calculations, special care should be taken when implementing this boundary condition. Indeed, the Dirac bispinor may be represented as

$$\varphi_{n\kappa m}(\mathbf{r}) = \frac{1}{r} \begin{pmatrix} P_{n\kappa}(r) \Omega_{\kappa m}(\hat{\mathbf{r}}) \\ i Q_{n\kappa}(r) \Omega_{-\kappa m}(\hat{\mathbf{r}}) \end{pmatrix}, \quad (7)$$

where P and Q are the large and small radial components, respectively, and Ω is the spherical spinor. The angular quantum number $\kappa = (l-j)(2j+1)$. The nonrelativistic boundary condition (6) applied directly to the above ansatz would lead to *two* separate constraints on P and Q. This overspecifies boundary conditions and leads to the Klein paradox.

A possible relativistic generalization of the boundary condition (6) is

$$\frac{d}{dr} \frac{P_{n\kappa}}{r}(R_{\mathrm{cav}}) = \frac{d}{dr} \frac{Q_{n\kappa}}{r}(R_{\mathrm{cav}}). \quad (8)$$

Since in the nonrelativistic limit the small component Q vanishes, this generalization subsumes Eq. (6). Due to the semiqualitative nature of our calculations, here we have chosen to use simpler (MIT bag model) boundary condition

$$P_{n\kappa}(R_{\mathrm{cav}}) = Q_{n\kappa}(R_{\mathrm{cav}}). \quad (9)$$

Nonrelativistically, it corresponds to an impenetrable cavity surface. Compared to this condition, the periodic boundary conditions (8) are "softer," i.e., they modify the free-atom wave functions less significantly; we expect that our use of Eq. (9) would somewhat overestimate the effects of confinement in the liquid.

Atom in a cavity: DHF and RRPA solutions. To reiterate the discussion so far, within the cell model, the complex liquid-structure problem is reduced to solving the atomic many-body Dirac equation with boundary conditions (9). The atomic-structure analysis is simplified by the fact that Xe is a closed-shell atom. Below we self-consistently solve the DHF equations inside the cavity. Then we employ more sophisticated RRPA.

At the DHF level, the atomic wave function is represented by the Slater determinant composed of occupied (core) orbitals φ_a. These orbitals are determined from a set of DHF equations

$$[c(\boldsymbol{\alpha} \cdot \mathbf{p}) + \beta c^2 + V_{\mathrm{nuc}} + V_{\mathrm{DHF}}] \varphi_a = \varepsilon_a \varphi_a, \quad (10)$$

where V_{nuc} is a potential of the Coulomb interaction with a finite-size nucleus of charge density $\rho_N(r)$ and V_{DHF} is a nonlocal self-consistent DHF potential. The DHF potential depends on all the core orbitals. Similar equations may be written for (virtual) excited orbitals φ_m.

We solved the DHF equations in the cavity using a *B*-spline basis set technique by Johnson *et al.* [14]. This technique is based on the Galerkin method: the DHF equations are expressed in terms of an extremum of an action integral

S_A. The boundary conditions are incorporated in the S_A as well. Furthermore, the action integral is expanded in terms of a finite set of basis functions (B splines). Minimization of such S_A with respect to expansion coefficients reduces solving integrodifferential DHF equations to solving a symmetric generalized eigenvalue problem of linear algebra. The resulting set of basis functions is finite and can be considered as numerically complete. In a typical calculation we used a set of basis functions expanded over 100 B splines.

Given a numerically complete set of DHF eigenfunctions $\{\varphi_i\}$, the permanent atomic EDM, Eq. (2), may be expressed as

$$\mathbf{d}^{\mathrm{DHF}} = 2\sum_{m,a} \frac{\langle\varphi_a|\mathbf{r}|\varphi_m\rangle\langle\varphi_m|h_{CP}|\varphi_a\rangle}{\varepsilon_m - \varepsilon_a}, \tag{11}$$

where a runs over occupied and m over virtual orbitals. Here h_{CP} is either a semileptonic interaction, Eq. (3), or an interaction with the nuclear Schiff moment, Eq. (4). An additional peculiarity related to the Dirac equation is an appearance of negative energy states ($\varepsilon_m < -m_e c^2$) in the summation over intermediate states in Eq. (11). We have verified that these states introduce a completely negligible correction to the computed EDMs.

To improve upon the DHF approximation, we have also computed EDMs using the RRPA method [15]. This approximation describes a dynamic linear response of an atom to a perturbing one-body interaction (e.g., H_{CP}). The perturbation modifies core orbitals, thus changing the DHF potential. This modification of V_{DHF} in turn requires the orbitals to adjust self-consistently. Such a readjustment process defines an infinite series of many-body diagrams, shown, e.g., in Ref. [7]. The RRPA series can be summed to all orders using iterative techniques or solving DHF-like equations. We used an alternative method of solutions based on the use of basis functions [16]. As an input, we used the DHF basis functions generated in the cavity (see discussion above), i.e., the boundary conditions were satisfied automatically. As a result of solving the RRPA equations, we have determined a quasicomplete set of particle-hole excited states and their energies. Then the EDMs are determined using expressions similar to Eqs. (1) and (2).

Discussion and conclusions. First, we present the results of our calculations for an isolated atom ($R_{\mathrm{cav}} = \infty$). For the Schiff-moment-induced EDM, our results, with $S = \boldsymbol{S}$,

$$d_{\mathrm{SM}}^{\mathrm{DHF}} = 2.88\left(\frac{S}{e\ \mathrm{fm}^3}\right) \times 10^{-18}\ e\ \mathrm{cm},$$

$$d_{\mathrm{SM}}^{\mathrm{RRPA}} = 3.78\left(\frac{S}{e\ \mathrm{fm}^3}\right) \times 10^{-18}\ e\ \mathrm{cm},$$

are in agreement with the recent calculations by Dzuba *et al.* [8]. For the EDM induced by T,P–odd semileptonic interactions we obtain

$$d_{\mathrm{TN}}^{\mathrm{DHF}} = 8.44 \times 10^{-13}\ C_{\mathrm{TN}} \sigma_N\ \mathrm{a.u.},$$

TABLE I. Individual contributions from various shells to the EDM of a free ^{129}Xe atom in the DHF and RRPA methods. The EDM is induced by the nuclear Schiff moment and it is given in units of $S/(e\ \mathrm{fm}^3) \times 10^{-18} e$ cm.

	DHF	RRPA
$n=1$	0.039	0.039
$n=2$	0.091	0.092
$n=3$	0.20	0.21
$n=4$	0.52	0.64
$n=5$	2.0	2.8
Total	2.88	3.78

$$d_{\mathrm{TN}}^{\mathrm{RRPA}} = 10.7 \times 10^{-13}\ \ C_{\mathrm{TN}}\ \sigma_N\ \mathrm{a.u.}$$

These values are to be compared with the results by Mårtensson-Pendrill [7], $d_{\mathrm{TN}}^{\mathrm{DHF}} = 7.764$, and $d_{\mathrm{TN}}^{\mathrm{RRPA}} = 9.808$ in the same units. The reason for the 10% difference between our results and those from Ref. [7] is not clear.

Before presenting results for finite cavity radii, let us consider individual contributions to EDM from various shells of Xe atom. These contributions for the Schiff-moment-induced EDM of an isolated atom are listed in Table I. A similar table, but for the EDM arising from semileptonic interactions is given in Ref. [7]. From these tables we observe that the dominant contribution to EDMs comes from the outer $n=5$ shell. Thus we anticipate that a noticeable density dependence should occur when R_{cav} becomes comparable to the size of external $n=5$ shell. We also notice that the contribution from the outer shell is relatively more important in RRPA calculations than at the DHF level, i.e., the RRPA results should exhibit stronger density dependence.

These qualitative conclusions for a confined atom are supported by our numerical results, presented in Fig. 1. Here we plot the ratios of atomic EDMs for the confined and isolated

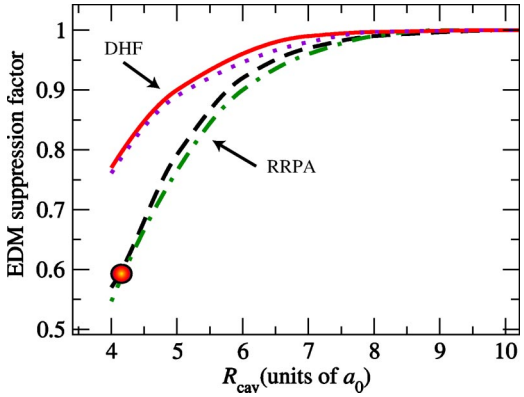

FIG. 1. The ratios of atomic EDMs for the confined and isolated atoms (suppression factor) as a function of cavity radius. The upper and lower sets of two curves are obtained with the DHF and RRPA methods, respectively. EDMs induced by P,T—odd semileptonic interactions are shown as solid and dashed lines, while EDMs due to the Schiff moment—as dotted and dashed-dotted lines. The heavy dot marks our final results for liquid Xe.

atoms as a function of R_{cav}. The EDMs become smaller as the density increases, $n \propto R_{cav}^{-3}$. At the density of liquid Xe, $R_{cav} \approx 4.9$ bohr, the more accurate RRPA results show a 25% suppression of the atomic EDM due to confinement. Overall there is a noticeable density dependence of atomic EDM. We expect the EDM signal (if found) to be broadened. The relevant characteristic width of the signal can be simply estimated from Fig. 1 from the mean density fluctuations.

From Fig. 1 we notice that both semileptonic– and Schiff–moment–induced EDMs scale with R_{cav} in a similar fashion. This similarity can be explained from the following arguments. The values of *CP*-violating matrix elements, Eqs.(3) and (4), are accumulated inside the nucleus. Nonrelativistically, as $r \to 0$ the wave functions scale as $\varphi_{nlm}(\mathbf{r}) \approx N_{nl}(R_{cav}) r^l Y_{lm}(\hat{\mathbf{r}})$, where N_{nl} are normalization factors. Therefore the dominant contribution to the EDM, Eq. (11) arises from mixing of *s* and *p* states. By factorizing the matrix element of h_{CP} as $\langle \varphi_{ns} | h_{CP} | \varphi_{n'p} \rangle \approx N_{ns}(R_{cav}) N_{n'p}(R_{cav}) \times \langle s | h_{CP} | p \rangle$ we see that the R_{cav}–independent factor $\langle s | h_{CP} | p \rangle$ can be pulled out of the summation over atomic orbitals in Eq.(11). Thus, both semileptonic– and Schiff–moment–induced EDMs exhibit approximately the same scaling with the cavity radius. A correction to this "similarity scaling law" may arise, for example, due to different selection rules involved for the two EDM operators.

It is worth emphasizing the semiqualitative nature of our calculations. The analysis can be improved by employing more realistic models of liquid environment. Even within the cell model we could further refine our analysis. A dense liquid may be considered as a solid with vacancies, i.e., the decrease of the average bond length is negligible, rather the nearest-neighbor occupation numbers are decreased compared to a solid. Xe condenses into face-centered cubic structure. The first nearest-neighbor shell contains 12 atoms (partially justifying the spherical symmetry of the elementary cell). The density of the solid Xe is 3.54 g/cm^3, implying the half-radius of this shell of 4.2 bohr, somewhat smaller than $R_{cav} \approx 4.9$ bohr for liquid Xe. As follows from Fig. 1, this difference leads to a more pronounced suppression of the atomic EDM by 40%.

To reiterate, our work was motivated by anticipated significant improvements in sensitivity to atomic EDMs in experiments with liquid ^{129}Xe [4]. Here we investigated confining effects of the environment on the EDM of a Xe atom. We carried out the analysis in the framework of the cell model coupled with relativistic atomic-structure calculations. We found that compared to an isolated atom, the EDM of an atom of liquid Xe is reduced by about 40%. Thus if the experiment with liquid Xe is carried out with the anticipated sensitivity, we expect that the inferred constraints on possible sources of *CP* violation would be indeed several orders of magnitude better than the present limits.

We would like to thank M. Romalis for discussions. This work was supported in part by the National Science Foundation.

[1] I. B. Khriplovich and S. K. Lamoreaux, *CP Violation Without Strangeness: Electric Dipole Moments of Particles, Atoms, and Molecules* (Springer, Berlin, 1997).

[2] E. N. Fortson, P. Sandars, and S. Barr, Phys. Today **56**(6), 33 (2003).

[3] M. V. Romalis, W. C. Griffith, J. P. Jacobs, and E. N. Fortson, Phys. Rev. Lett. **86**, 2505 (2001).

[4] M. V. Romalis and M. P. Ledbetter, Phys. Rev. Lett. **87**, 067601 (2001).

[5] M. A. Rosenberry and T. E. Chupp, Phys. Rev. Lett. **86**, 22 (2001).

[6] V. L. Varentsov, V. G. Gorshkov, V. F. Ezhov, M. G. Kozlov, L. N. Labzovskii, and V. N. Fomichev, Pis'ma Zh. Eksp. Teor. Fiz. **36**, 141 (1982) [JETP Lett. **36**, 175 (1982)].

[7] A. Mårtensson-Pendrill, Phys. Rev. Lett. **54**, 1153 (1985).

[8] V. Dzuba, V. Flambaum, J. Ginges, and M. Kozlov, Phys. Rev. A **66**, 012111 (2002).

[9] L. I. Schiff, Phys. Rev. **132**, 2194 (1963).

[10] V. Flambaum and J. Ginges, Phys. Rev. A **65**, 032113 (2002).

[11] S. H. Patil, J. Phys. B **35**, 255 (2002).

[12] Amagat density unit is equal to 44.615 moles per cubic meter (mol/m^2).

[13] P. Stampfli and K. H. Bennemann, Phys. Rev. A **44**, 8210 (1991).

[14] W. R. Johnson, S. A. Blundell, and J. Sapirstein, Phys. Rev. A **37**, 307 (1988).

[15] A. L. Fetter and J. D. Walecka, *Quantum Theory of Many-particle Systems* (McGraw-Hill, New York, 1971).

[16] W. R. Johnson, Adv. At. Mol. Phys. **25**, 375 (1988).